THE JOURNAL OF BIOLOGICAL CHEMISTRY
Vol. 270, No. 25, Issue of June 23, pp. 15194–15202, 1995
Printed in U.S.A.

Structure of Human Parathyroid Hormone 1–37 in Solution*

(Received for publication, February 5, 1995, and in revised form, April 12, 1995)

Ute C. Marx, Sabine Austermann‡, Peter Bayer, Knut Adermann‡, Andrzej Ejchart, Heinrich Sticht, Stefan Walter§, Franz-Xaver Schmid§, Rainer Jaenicke¶, Wolf-Georg Forssmann‡, and Paul Rösch‖

From the §Lehrstuhl für Biochemie, Universität Bayreuth, D-95440 Bayreuth, the ‡Niedersächsisches Institut für Peptid-Forschung GmbH, Feodor-Lynen-Strasse 31, D-30625 Hannover, and the ¶Institut für Biophysik und Physikalische Biochemie, Universität Regensburg, D-93053 Regensburg, Federal Republic of Germany

Human parathyroid hormone (hPTH), amino acids Ser[1] to Leu[37], is biologically active with respect to both receptor binding and activation of adenylate cyclase to influence the serum calcium concentration. It induces DNA synthesis via an unknown signal pathway. We investigated the structure of hPTH(1–37) in H_2O/buffer solution under near physiological conditions, that is pH 6.0 and 270 mM salt, by circular dichroism, ultracentrifugation, nuclear magnetic resonance spectroscopy, and molecular dynamics calculations. Complete sequence specific assignments of all ^1H resonances were performed by using ^1H two-dimensional NMR measurements (double quantum-filtered correlated spectroscopy, nuclear Overhauser effect spectroscopy (NOESY), and total correlation spectroscopy with suppression of NOESY-type cross-peaks spectra). hPTH(1–37) obtained helical structure and showed hydrophobic interactions defining a tertiary structure. The NH_2-terminal four amino acids of hPTH(1–37) did not show a stable conformation. Evidence for an α-helical region between Ile[5] and Asn[10] was found. This region was followed by a flexible link (Gly[12], Lys[13]) and a well defined turn region, His[14] to Ser[17]. The latter was stabilized by hydrophobic interactions between Trp[23] and Leu[15]. Ser[17] through at least Leu[28] formed an α-helix. Arg[20] and Lys[27] were involved in the core built by His[14] to Ser[17]. Unrestrained molecular dynamics simulations indicated that the structure was stable on the 200 ps time scale.

Human parathyroid hormone (hPTH)[1] contains three functionally distinct domains that are responsible for receptor binding and activation of cAMP-cyclase to maintain normocalcaemia and initiation of a cAMP-independent signal transduction pathway for stimulation of DNA synthesis, respectively (1, 2). It is generally accepted that these functionally active domains of the 84 amino acid hormone are located in the NH_2-terminal part of the protein (3). Indeed, hPTH(1–37) (for sequence, see Table I) is the naturally occurring bioactive hormone extractable from human blood (4). The cAMP receptor-binding domain comprises His[14] to Phe[34] (5, 6), and the DNA synthesis stimulating domain comprises Asp[30] to Phe[34] (1). The complete NH_2-terminal peptide hPTH(1–34) is required for stimulation of the cAMP-dependent signal pathway (3). Stimulatory potential is lost on deletion of Ser[1] and Val[2]. cAMP-receptor binding capacity is not influenced by this deletion, indicating that the activation and receptor-binding sites are located in different domains (7). The intact cAMP-dependent signal pathway is required to maintain normocalcaemia. Moreover, treatment of osteoporotic patients with hPTH hormone stimulates an increase of axial bone mass and bone formation (8). Thus, recent studies focused on determination of the three-dimensional structure of NH_2-terminal peptides in solution by NMR spectroscopy. In particular, hPTH(1–34) is an intensely studied hormone fragment. It contains the functional domains and, in addition, is commercially available in large quantities as necessary for solution structural studies by NMR spectroscopy ((9–11); for a recent review, see Ref. 12). The results of these studies are still under discussion, as the majority concludes that hPTH(1–34) does not form secondary structure elements under near physiological solvent conditions (9, 11, 13), but helix formation under these conditions is also observed (10). In 2,2,2-trifluoroethanol (TFE) containing solution, however, helical structure is induced (9, 11, 13). In particular, in 40% TFE solution, hPTH(1–34) displays helical regions from Ser[3]3 to Gly[12] and from Ser[17] to Lys[26] (11). In 70% TFE, hPTH(1–34) showed similar behavior (13).

Contrasting these studies of hPTH(1–34) in TFE-containing solution is NMR work on the same fragment and on human parathyroid hormone-related protein in H_2O solution (14, 15). These studies claim that the NH_2-terminal peptide of hPTH obtains stable α-helical structure in H_2O solution from Glu[4] to Lys[13] and Val[21] to Gln[29].

TFE is commonly used as an additive to protein and peptide solutions that stabilizes secondary structures, in particular α-helices (16–21). It is also used to stabilize putative protein folding intermediates (22). Being mildly hydrophobic with a dielectric constant $\epsilon = 26.7$, that is one-third that of water (23), TFE bears the risk of weakening hydrophobically stabilized tertiary structure domains (19).

Thus, on one hand, the structural results on hPTH(1–34) are at least partially contradictory. On the other hand, determination of the three-dimensional structure of the NH_2-terminal

* This work was supported by grant sFB213, D8 from the Deutsche Forschungsgemeinschaft and by grants from the the Fonds der Chemischen Industrie (FCI) (to P. R.), the Graduiertenkolleg Biosynthese der Proteine und Regulation ihrer Aktivität (to U. C. M.), the FCI (to H. S.), and a FCI Kekulé fellowship (to P. B.). The costs of publication of this article were defrayed in part by the payment of page charges. This article must therefore be hereby marked "*advertisement*" in accordance with 18 U.S.C. Section 1734 solely to indicate this fact.

The atomic coordinates and structure factors (code 1HPH) have been deposited in the Protein Data Bank, Brookhaven National Laboratory, Upton, NY.

‖ To whom correspondence should be addressed: Lehrstuhl für Biopolymere, Universität Bayreuth, 95440 Bayreuth, Germany. Tel.: 49 921 55 35 40; Fax: 49 921 55 35 44; E-mail: paul.roesch@unibayreuth.de.

[1] The abbreviations used are: hPTH, human parathyroid hormone; CLEAN-TOCSY, TOCSY with suppression of NOESY-type cross-peaks; COSY, correlated spectroscopy; DQF-COSY, double quantum filtered COSY; Fmoc, 9-fluorenyl methyl oxycarbonyl; HPLC, high performance liquid chromatography; PTH, parathyroid hormone; NOE, nuclear Overhauser effect; NOESY, NOE spectroscopy; TBTU, 2-(1H-benzotriazol-1-yl)-1,1,3,3-tetramethyluronium tetrafluoroborate; TFE, 2,2,2-trifluoroethanol; TOCSY, total correlation spectroscopy; rmsd, root mean square deviation.

part of hPTH poses a problem of considerable medical and pharmaceutical importance, as drugs mimicking this structure might eventually be extremely useful as therapeutics against osteoporosis and parathyroid gland malfunction or loss.

hPTH(1–37) is not only the naturally occurring hPTH fragment extractable from human blood, but also shows higher cAMP generation activity in target cells than hPTH(1–34) (4). Compared to hPTH(1–34), hPTH(1–37) is extended by Val, Ala, and Leu. Ala is a strong helix stabilizer (24), and the structure of hPTH in the region Asp^{30}-Phe^{34} is stabilized by flanking amino acids (1). On these grounds we decided to study the hPTH NH_2-terminal fragment 1–37 in aqueous solution under conditions approaching the physiological state with respect to salt concentration and pH, and compare the results with the structures obtained earlier for hPTH(1–34) in TFE-containing solution.

MATERIALS AND METHODS

Peptide Synthesis—hPTH(1–37) was synthesized on an automated peptide synthesizer (Millipore) 9050 using standard Fmoc protocols with Fmoc-Arg(PMC) and Fmoc-Trp(Boc) (25). Peptide chains were assembled by TBTU/DIPEA/HOBT activation on preloaded PEG-PS resin (Millipore). Cleavage and deprotection reactions were performed with trifluoroacetic acid/ethandithiole/water (94:3:3) for 90 min. The peptide was precipitated by addition of cold *tert*-butylmethylether, dissolved in 5% acetic acid for 15 h, and lyophilized. The crude product was purified by reverse phase (RP) HPLC (Vydac C18, 10 μ, 25 mm × 250 mm, 10 ml/min, 230 nm, buffer A: 0.1% HCl, buffer B: 0.1% HCl in PrOH/MeOH/water 50:30:20 with a constant gradient of 10–70% B in 60 min). Purity was checked with RP-HPLC (Vydac C18, 250 × 4.6 mm, 300 A, 10 m) and capillary zone electrophoresis (Biofocus 3000, Bio-Rad). Electrospray mass spectrometry (Sciex API III, Perkin-Elmer) showed correct relative molecular mass (calculated: 4401.01; measured: 4401 ± 1). Automated Edman degradation (473A Protein sequencer, Applied Biosystems) and amino acid analysis (Aminoquant 1090L, Hewlett Packard) confirmed amino acid composition as well as amino acid sequence. The lyophilized product was stored at −20 °C.

Biological Activity—Biological activity of the synthetic hPTH(1–37) fragment was tested by observation of the stimulation of cAMP generation in osteogenic cells (Rous sarcoma cells) and in an established renal epithelial cell line (opossum kidney cell).[2]

Sedimentation Analysis—Sedimentation experiments were performed at room temperature in a Beckman model E analytical ultracentrifuge, using UV scanning at 280, 290, 295 and 300 nm. Double sector cells with sapphire windows were applied in an AnH-Ti rotor. The $s_{20,w}$ value was calculated from a lg(*r*) *versus* time plot, correcting for temperature and water viscosity; high speed sedimentation equilibria (26) were evaluated from ln(*c*) *versus* r^2 plots making use of a computer program developed by G. Böhm, Regensburg. The partial specific volume of the protein was calculated from the amino acid composition.

NMR Spectroscopy—NMR spectra were obtained on a standard Bruker AMX600 spectrometer at 283 K and 298 K with standard methods (27, 28). Advantages in lineshape and linewidth led us to use ~3.4 mM protein in 50 mM potassium phosphate buffer with ~270 mM sodium chloride, pH 6.0. The H_2O resonance was presaturated by continuous coherent irradiation at the resonance frequency prior to the reading pulse. Differences in sample heating between TOCSY spectra and other spectra were compensated for by temperature calibration of the probe for the specific buffer system and accordingly corrected presettings for the VT1000 temperature unit. The sweep widths in ω_1 and ω_2 were identical, 7042.3 Hz and 6024.1 Hz for the spectra obtained in $H_2O/^2H_2O$ (9:1) and ^2H_2O solution, respectively. Quadrature detection was used in both dimensions, employing the time proportional phase incrementation technique in ω_1. 4 K data points were collected in ω_2 and 512 data points were collected in ω_1. Zero filling to 1 K and 2 K data points, respectively, was used in ω_1 and ω_2. For determination of J-couplings, zero filling to 16 K in ω_2 was used. All two-dimensional spectra were multiplied by a squared sinebell function phase shifted $\pi/4$ for NOESY spectra, $\pi/6$ for TOCSY spectra, and $\pi/8$ for COSY spectra. Base line and phase correction to 6th order was used. Data were evaluated on X-window workstations with the NDee program package (available to non-profit organizations on request).

Data from the following 600 MHz NMR spectra were employed for the sequence-specific assignment of spin systems and the evaluation of NOESY distance constraints: DQF-COSY, TOCSY with mixing times of 70 and 80 ms, respectively, NOESY with mixing times of 100 and 200 ms, respectively. NOESY cross-peaks were obtained from two sets of spectra at 283 and 298 K. For the present calculations, only NOEs visible in the 298 K spectra with 200 ms mixing time were taken into account, although identical calculations combining information obtained at the two different temperatures resulted in identical structures.

CD Spectroscopy—CD spectra were recorded at 25 °C in 0.1-mm cells from 250 to 190 nm at 20 nm/min on a Jasco J 600A CD spectropolarimeter with 310 μM protein in pH 6.0 solution containing 270 mM sodium chloride and 50 mM phosphate buffer in 30 μl volume. The reference sample contained buffer without protein. Spectra were measured eight times and averaged for sample and reference, respectively.

Structure Calculations with Restrained Molecular Dynamics—Distance geometry (DG) and molecular dynamics (MD) calculations were performed with the XPLOR 3.1 program package (29) on CRAY Y-MP/EL and HP735 computers. 520 NOESY cross-peaks could be assigned, of which 183 were structure determining interresidual cross-peaks (560 and 223 cross-peaks, respectively, when combining the cross-peaks from the sets of spectra obtained at 283 K and 293 K). We divided these cross-peaks into three groups according to their relative intensities: strong intensity, 0.2–0.3 nm, medium intensity, 0.2–0.4 nm, and weak intensity, 0.2–0.5 nm. 0.05 nm was added to the upper distance limit for distances involving unresolved methyl or methylene proton resonances (pseudoatom approach).

The structure calculations followed standard procedures employing a hybrid DG-restrained MD approach with simulated annealing (SA) refinement and subsequent energy minimization (dgsa; (29)). For the refinement, the dielectric constant was changed to $\epsilon = 4$. Structure parameters were extracted from the standard parallhdg.pro and topallhdg.pro parameter files (30).

Unrestrained MD—Unrestrained MD calculations were carried out using the parameters for the polypeptide chain and the TIP3P water model (31) that were supplied with the standard X-PLOR force field (29). A representative structure out of 30 structures calculated as above was chosen as starting structure for the unrestrained MD calculations.

A cubic water box consisting of 8000 water molecules with a length of 6.22 nm in each dimension was set up, based on an equilibrated box of 125 water molecules as supplied with the X-PLOR program package. The overlay was achieved by placing the protein in the center of the water box and by deleting all solvent molecules closer than 0.26 nm to any heavy atom of the protein.

Close Nonbonded Solute-Solvent Interactions Were Removed in Two Steps—First, 100 cycles of conjugate gradient energy minimization (32) were carried out, keeping the positions of all protein atoms fixed. Second, in 300 cycles of energy minimization, a harmonic potential was used to restrain the peptide to its original conformation.

During the first 15 ps of the MD calculations, the system was gradually heated to 300 K while coupled to an external water bath (33). The MD calculations were carried out using the Verlet algorithm (34) with a time step of 2 fs. The SHAKE facility (35) was used to constrain the covalent bond length. A dielectric constant of 1.0 was applied with a scaling factor of 0.4 for one to four electrostatic interactions. All nonbonded interactions were cut off at a distance of 0.85 nm.

The heating stage was followed by 200 ps of MD at 300 K using the parameters described above. During the whole simulation minimum image periodic boundary conditions were used. Coordinates, energies, and velocities were saved every 5 ps for further analysis.

Simulations and analyses were performed on Cray YMP/EL and Hewlett Packard HP 735 computers. A 1 ps simulation required about 2 h of cpu time on a Cray YMP/EL computer.

Structural Analysis—The final structures were analyzed with respect to stable idealized elements of regular secondary structure using the Determination of Secondary Structure of Proteins (DSSP) program package (36). For visualization of structure data, the SYBYL program package, version 6.0, (TRIPOS Association) was used.

RESULTS AND DISCUSSION

Molecular Mass—From sedimentation velocity experiments at 68,000 revolutions/min, a sedimentation coefficient $s_{20,w}$ = 0.51 ± 0.02 S was obtained, in accordance with a globular protein of less than 5 kDa molecular mass; boundary analysis provided clear evidence for homogeneity. High speed sedimentation equilibria at 40,000 and 30,000 revolutions/min gave

[2] W.-G. Forssmann and D. Hock, personal communication.

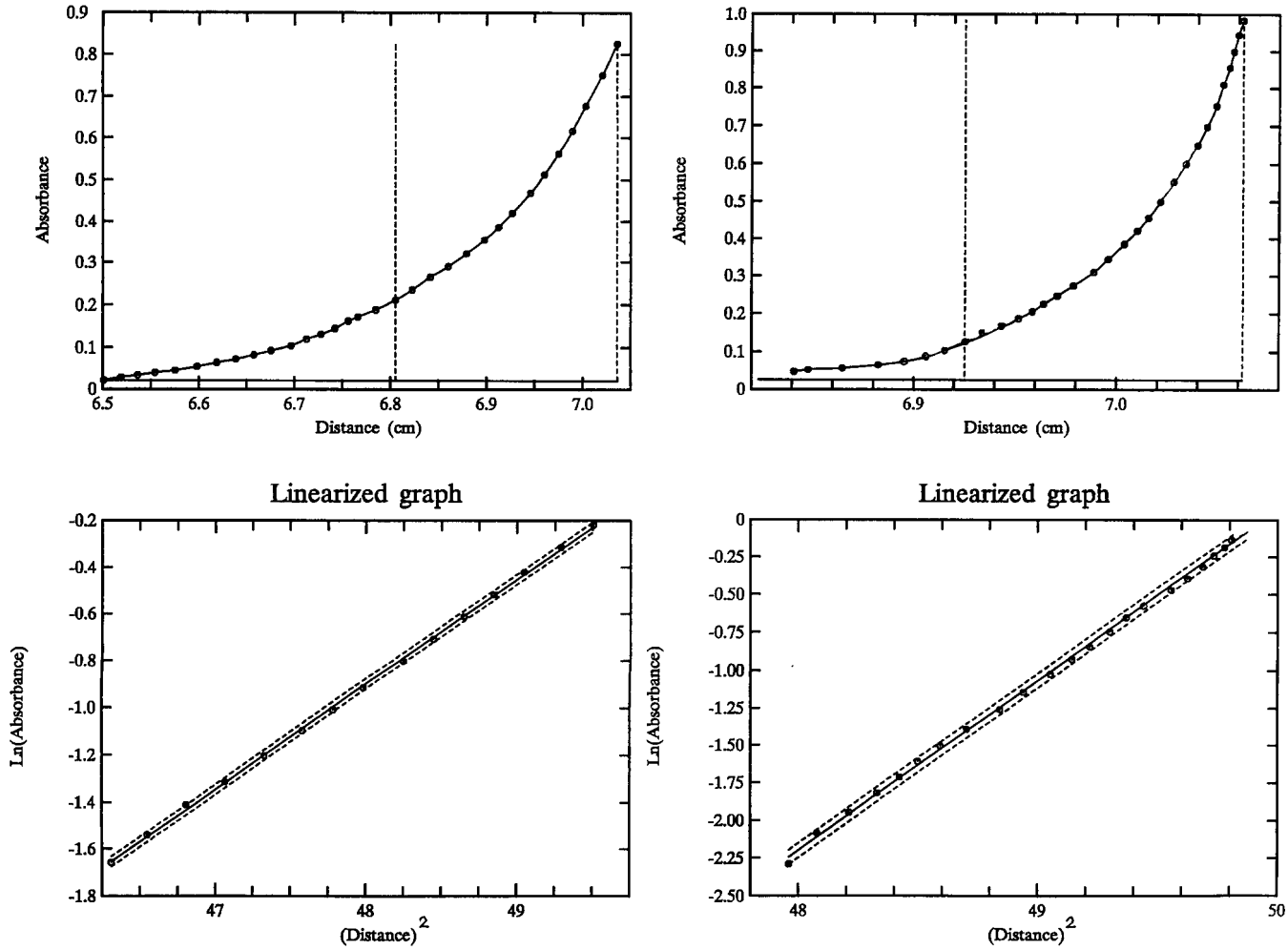

FIG. 1. **Ultracentrifugal analysis of parathyroid hormone in 50 mM potassium phosphate, pH 6.3, at 20 °C, initial peptide concentration 0.35 mg/ml.** Meniscus depletion high speed sedimentation equilibrium at 40,000 (*left*) and 68,000 revolutions/min (*right*). *Upper panels*, radial distribution (*c versus r*), scanned at 280 nm. *Lower panels*: ln*c versus* r^2 linearization of the bottom region yield the monomer molecular mass of 4,390 ± 228 and 4 105 ± 17 Da for 40,000 and 68,000 revolutions/min, respectively.

linear ln *c versus* r^2 plots from which a molecular mass of 4,105 ± 175 was calculated (correlation coefficient 0.9994) (Fig. 1). In order to detect possible concentration-dependent association, heterogeneity, and nonideality, the meniscus depletion technique (26) was applied. Using scanning wavelengths between 280 and 300 nm, the maximum concentration at the bottom of the cell was extended to 24 mg/ml. No tendency to form dimers or high molecular weight aggregates could be detected. One-dimensional NMR spectra of hPTH(1–37) were identical in a concentration range from 0.04 3.4 mM (data not shown), confirming that hPTH(1–37) did not form aggregates at the concentrations used for further NMR experiments.

Circular Dichroism Spectroscopy—The overall content of helical structure elements was determined by far UV CD spectroscopy (Fig. 2). The evaluation of the average helix content of the peptide by two standard methods (37, 38) yielded an average helix content of hPTH(1–37) of 28–30%.

Two-dimensional NMR Spectroscopy—The two-dimensional NMR spectra of hPTH(1–37) showed very little resonance overlap (Fig. 3), so that the sequence-specific resonance assignments could be performed with standard techniques (28). The complete NH-C_αH resonance assignments are shown in the 200 ms NOESY spectrum (Fig. 3*b*), and the complete sequence-specific resonance assignments are given in Table I.

The high number of cross-peaks in the backbone amide-amide region of the NOESY spectra (Fig. 3*a*) immediately

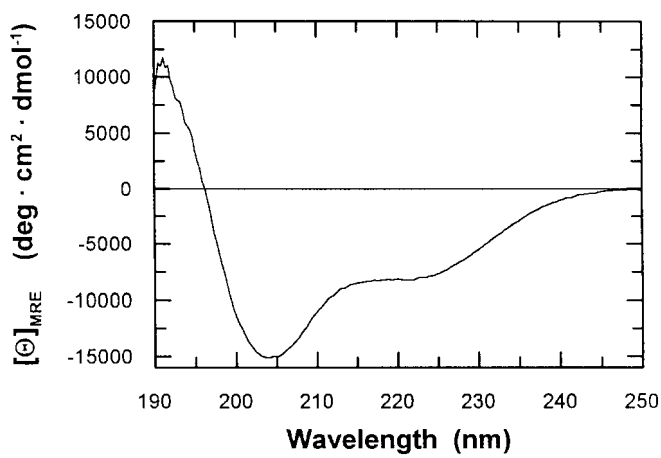

FIG. 2. **Far UV circular dichroism spectrum of hPTH(1–37) as under "Materials and Methods."** The presence of approximately 30% helical structure may be estimated from this CD spectrum.

suggested the presence of helical structures. We used the chemical shift data available from our experiments to perform a secondary structure estimate according to the chemical shift index strategy (39). The procedure depends on a simple correlation between chemical shifts of C_α-proton resonances of consecutive amino acids and local secondary structure: C_α proton

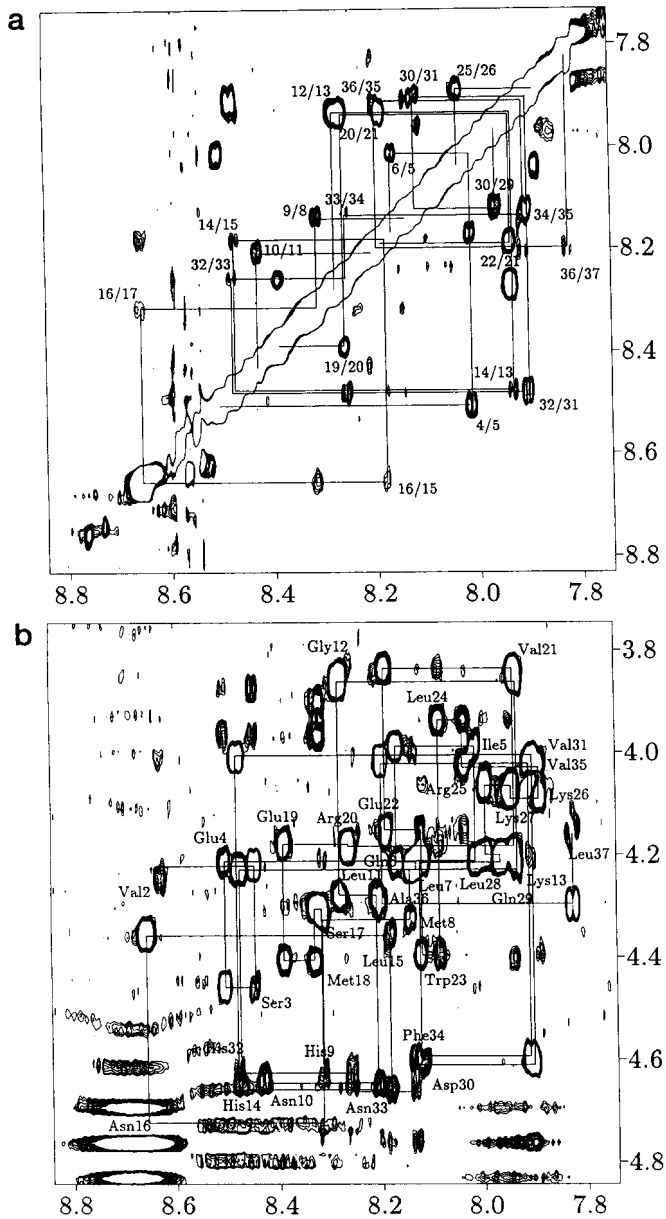

FIG. 3. **200 ms NOESY spectrum of hPTH(1–37).** *a*, amide-amide region; *b*, fingerprint region. Experimental conditions: NMR: mixing time, 200 ms; data size: 4 k × 1 k data points; filter: squared sine bell, phase shift $\pi/4$; ns, 96. Sample conditions: hPTH, 1.8 mM; pH, 6.0; T, 298 K; NaCl, 250 mM; potassium phosphate, 50 mM.

resonances shifted to high field relative to the corresponding random coil C_α proton resonances indicate local α-helical structure; C_α proton resonances shifted downfield compared to the corresponding resonances in a random coil structure indicate local β-sheet structure. The criterion for taking a particular shift into account in secondary structure estimates is its deviation from the random coil value by more than 0.1 parts/million. Also, to get a more reliable picture, it is suggested that only resonances should be taken into account with the same sense chemical shift deviation for a stretch of more than 3 sequential residues (39). This procedure results in surprisingly accurate estimates (40–42). For hPTH(1–37), chemical shift indexing indicated a helical region extending from Met^{18} to Lys^{27}, and a shorter helical region around Leu^7 (Fig. 4). No other elements of regular secondary structure were suggested by this procedure.

This preliminary estimate was corroborated by the detection of C_αH-NH(i,i+3) and C_αH-C_βH(i,i+3) NOESY cross-peaks (Fig. 5). From the (i,i+3) cross-peak pattern, it is suggested that the peptide has a propensity to form helical regions from Ile^5 to Asn^{10} and from Met^{18} to at least Asp^{30}. The C_αH-NH (i,i+3) cross-peak pattern may be interpreted to indicate that this region extends to Phe^{34}.

The dgsa protocol employed for structure determination yielded the energy values shown in Table II. Superposition of 10 backbone structures, His^{14} to Leu^{28}, resulting from this procedure showed that the structure was well defined in this sequence region (Fig. 6*a*). A single structure selected from this group of structures clearly displayed the secondary structure elements and the formation of tertiary structure around the His^{14} to Ser^{17} turn region (Fig. 6*b*). From the NH_2 terminus, the first regular secondary structure element was a single helix turn, Ile^5 to His^9. The second α-helix was experimentally well defined by helix type intermediate range NOEs from Ser^{17} to Leu^{28}. This helix extended to Asp^{30} during the first 5 ps of an unrestrained molecular dynamics calculation. A flexible region through the COOH terminus followed. The very NH_2 and COOH termini were not fixed by long range NOESY cross-peaks. A turn structure, His^{14} to Ser^{17}, was defined by 23 interresidual NOESY cross-peaks in this region. This turn was probably stabilized by hydrophobic interactions involving Leu^{15} and Trp^{23}, among others. Experimentally, the relative position of these two amino acids was fixed by five long range NOESY cross-peaks. Furthermore, 13 NOESY cross-peaks between Trp^{23} and Lys^{27}, four NOESY cross-peaks between Trp^{23} and Arg^{20}, and six NOESY cross-peaks between Leu^{15} and Arg^{20} defined the tertiary fold. This observation of tertiary interactions was corroborated by the set of spectra obtained at 283 K. Taking into account information at both temperatures, the total number of interresidual NOEs defining the turn region increased to 31, and the total number of interresidual NOEs between Leu^{15} and Trp^{23} to six. These direct observations of tertiary interactions clearly lent further support to the results of the restrained molecular dynamics calculations that were based on the 298 K data only.

Stability of Structure—Small linear peptide fragments usually display a higher amount of flexibility than globular proteins, that is they populate a whole range of conformations (43). A general problem of structural NMR studies of flexible molecules is the very nature of the observed NOE data as a population weighted average. Thus, in particular in peptide studies, additional information from other sources, spectroscopic and computational, is needed to further characterize the dynamic state of the system (43). Suggestions have been made to resolve this situation with restrained molecular dynamics methods (44), but these procedures are not yet applied widely.

In the current study, only conservative semiquantitative NOE intensity based estimates of interproton distances were used for the restrained molecular dynamics calculations. Although this procedure weakens the danger of overinterpretation of experimental data, it does not remove it entirely.

The stability of the tertiary and secondary structure presented here may be judged in various ways. First, relative NOE intensities may be compared with results from other peptides and proteins; second, for a purely helical peptide, the amount of helices present at any given point in time may be estimated from the CD spectra; third, local rmsd values may be calculated; fourth, the structural stability may be probed by unrestrained molecular dynamics calculations, and the time dependence of the structural elements may be followed.

Relative NOE Intensities—The geometry of an idealized α-helix suggests that the backbone atom distances $dC_{\alpha N}(i,i+1)$ and $dC_{\alpha N}(i,i+3)$ are very similar to each other, whereas

TABLE I
^1H chemical shifts and assignments for hPTH(1–37) at pH 6.0, 298 K, 250 mM NaCl relative to DSS as an external standard, accuracy +/− 0.01 parts/m

Residue	NH	Hα	Hβ	Hγ	Others
Ser[1]		4.25	4.02		
Val[2]	8.63	4.22	2.11	0.97	
Ser[3]	8.45	4.46	3.96/3.87		
Glu[4]	8.51	4.21	2.02	2.30	
Ile[5]	8.02	3.99	1.84	1.48/1.20/0.87	0.85
Gln[6]	8.17	4.21	2.07	2.37	7.52/6.89(NH_2)
Leu[7]	8.13	4.23	1.67	1.57	0.89/0.84(δ)
Met[8]	8.14	4.33	2.03	2.60/2.49	
His[9]	8.32	4.63	3.30/3.20		8.45(2); 7.22(4)
Asn[10]	8.43	4.65	2.86/2.81	7.62/6.95(NH_2)	
Leu[11]	8.21	4.28	1.70	1.60	0.89/0.84(δ)
Gly[12]	8.28	3.86			
Lys[13]	7.93	4.23	1.69	1.33	1.63(δ); 2.95(ε)
His[14]	8.48	4.66	3.25/3.15		8.43(2); 7.17(4)
Leu[15]	8.18	4.36	1.61	1.52	0.78(δ)
Asn[16]	8.66	4.73	2.95/2.87	7.60/6.94(NH_2)	
Ser[17]	8.32	4.31	3.97/3.90		
Met[18]	8.33	4.41	2.10	2.55/2.64	
Glu[19]	3.39	4.18	2.05	2.29/2.39	
Arg[20]	8.26	4.18	1.82/1.91	1.58/1.67	3.15(δ); 7.24(ε)
Val[21]	7.94	3.84	2.14	1.02/0.89	
Glu[22]	8.19	4.15	2.07	2.32	
Trp[23]	8.12	4.40	3.41/3.32		10.18(1NH); 7.25(2); 7.55(4); 7.08(5); 7.19(6); 7.47(7)
Leu[24]	8.09	3.94	1.72	1.57	0.89(δ)
Arg[25]	8.04	4.03	1.87	1.58/1.71	3.17(δ); 7.36(ε)
Lys[26]	7.89	4.09	1.79	1.38/1.49	1.64(δ); 2.95(ε)
Lys[27]	7.95	4.07	1.58/1.66	1.15	1.48(δ); 2.84/2.78(ε)
Leu[28]	8.00	4.20	1.69	1.55	0.85(δ)
Gln[29]	7.97	4.22	2.05	2.39	7.50/6.84(NH_2)
Asp[30]	8.12	4.61	2.75/2.65		
Val[31]	7.90	4.01	2.08	0.85	
His[32]	8.48	4.63	3.22/3.13		8.50(2); 7.18(4)
Asn[33]	8.26	4.66	2.74/2.67	7.60/6.88(NH_2)	
Phe[34]	8.14	4.59	3.06		7.21(2,6); 7.27(3,5); 7.30(4)
Val[35]	7.91	4.02	1.96	0.88	
Ala[36]	8.20	4.30	1.37		
Leu[37]	7.83	4.16	1.57		0.84/0.88(δ)

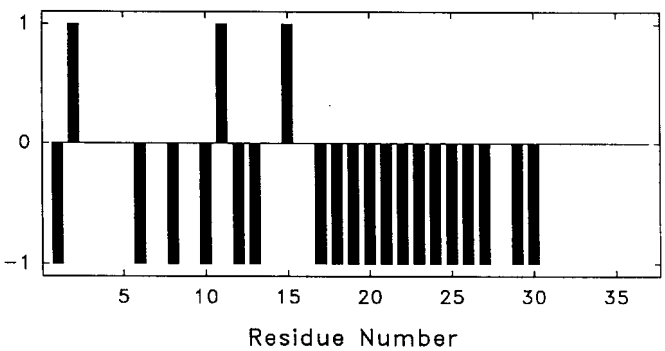

FIG. 4. **Chemical shift diagram according to (Ref. 39) as described in the text.**

$d_{NN}(i,i+1)$ distances are appreciably shorter (approximately 0.35 *versus* 0.28 nm; (45, 46)). Distances involving side chain C_β protons may occupy a wider range of distances in α-helices ($dC_{\alpha\beta}(i,i+3)$ = 0.25 − 0.44 nm, $dC_{\beta N}(i,i+1)$ = 0.25 − 0.41 nm (28)). Consequently, the ratio of these intensities may be used as a qualitative estimate of the fractional helix content of specific sequence regions. In the dimerization stabilized α-helix of the GCN4 leuzine zipper, the intensity of several classes of these NOESY cross-peaks is of comparable magnitude in some studies (47–49). The same is true for typical zinc-finger α-helices that are stabilized by the divalent metal ion and related motifs (50–53). Nascent helix structures (54) do not show $i,i+3$ NOESY cross-peaks, and the basic domain-leucine zipper motif basic DNA-binding domain of GCN4 (55) may be considered an example of this type of nascent helix structure. Absence or very low intensity of $i,i+3$ cross-peaks is also observed in studies of some leucine zipper motifs, for example the Jun oncoprotein homodimer (56). From this comparison of NOESY cross- peaks, the helical regions of hPTH(1–37) in TFE-free solution showed a fractional helix content similar to the zinc-finger and the more stable category of leucine zipper α-helices. Appearance of strong $\alpha N(i,i+1)$ cross-peaks in the helices of hPTH(1–37) indicated contribution of some extended conformation even in these structured regions. Direct quantitative estimate, however, of fractional helix content for PTH(1–37) based on the present NMR data is not possible.

CD Spectroscopy—Estimates of the secondary structure content of hPTH(1–37) based on published procedures (37, 38) indicated 28–30% helical structure. This corresponds to 11 amino acids employed in perfectly stable regular secondary structure or, alternatively, to more than 11 amino acids involved in weaker, transient helix formation. Secondary structure determination by NMR and NOE-based restrained molecular dynamics calculations suggested that Gln[6] to His[9] and Ser[17] to Leu[28] formed helical structures according to structure analysis with the DSSP program package (36). Assuming that the length of the helices is reflected correctly by this procedure, the CD measurements showed that the helical sequences in hPTH were in helical conformation in 70% of the time on average. Judging this result, one has to take into account the low sensitivity of CD spectroscopy with respect to the determination of helices less than 6 amino acids in length. It is believed that 4 amino acid helices result in CD spectra that clearly deviate from the ideal helix type spectra, but these matters are still under discussion ((57, 58) and literature cited therein). Thus, a time average of 70% for the presence of helices in

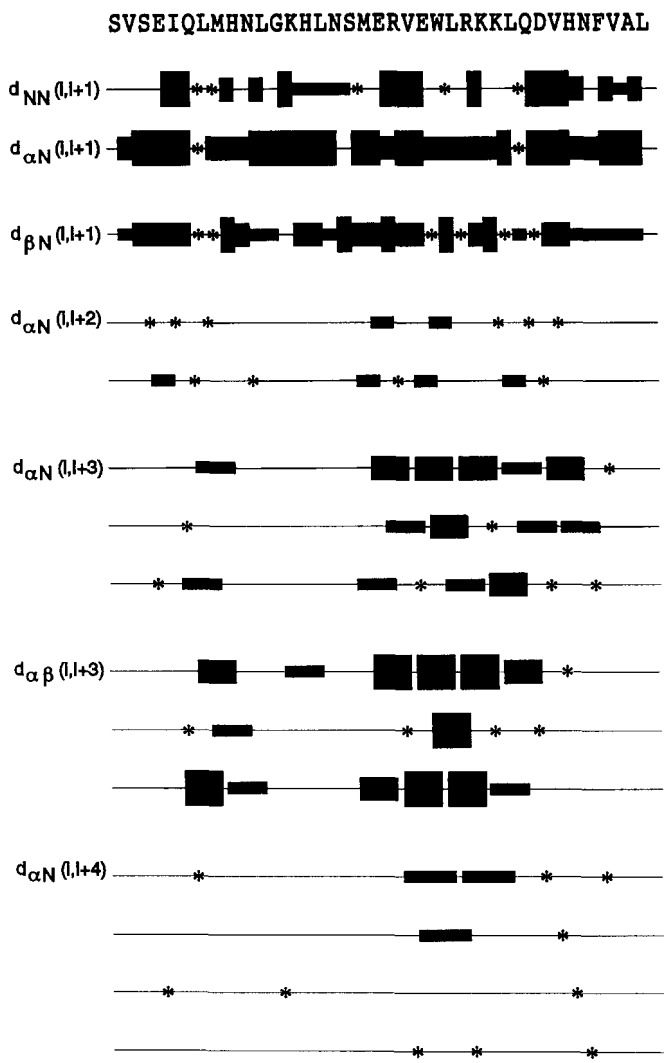

FIG. 5. **NOEs *versus* sequence.** The thickness of the bars qualitatively indicates the relative strength of the NOESY cross-peaks. An *asterisk* indicates that the NOE could not be observed because of frequency degeneration.

hPTH(1–37) clearly is a conservative lower limit of the time averaged formation of helices in the two hPTH regions Gln^6 to His^9 and Ser^{17} to Leu^{28}.

Local rmsd Values—The superposition of the helical structure of hPTH(1–37) resulted in a comparatively low rmsd value. This indication of helix stability is confirmed by calculating local rmsd values (59). The latter showed a very marked decrease in the helical regions (Fig. 7).

Unrestrained Molecular Dynamics—Unrestrained MD calculations of the hPTH(1–37) peptide in H_2O were performed to probe the structural stability of the two helical regions determined by NMR and restrained MD calculations, that is Gln^6 to His^9 and Ser^{17} to Leu^{28}. The 200 ps simulation calculations clearly showed that the extent of the helical conformation was slightly increasing, and the helical regions were from Ile^5 to Asn^{10} and Ser^{17} to Asp^{30}/Val^{31} for most of the time. The local formation of α-helices proved to be stable as shown by a diagram of helix length *versus* time (Fig. 8*b*). The rmsd value of the backbone and side chain heavy atoms of the structures in the unrestrained molecular dynamics calculation as compared to the starting structure increased only slightly at the very beginning of the calculation, as expected, and remained stable for the remaining period (Fig. 8*a*). Earlier 200 ps simulations of this type performed on α-helix H8-HC5 of myoglobin (residues 132–153) showed that this helix is stable in TFE, whereas it is unstable in H_2O on this time scale (60), validating the MD approach to peptide stability characterization. Comparison of the results of our unrestrained MD calculations on hPTH(1–37) with those on α-helix H8-HC5 of myoglobin clearly show that the latter is much less stable in H_2O on this time scale (60). Furthermore, the unrestrained molecular dynamics simulations on hPTH(1–37) also showed that the small hydrophobic core formed by Leu^{15} and Trp^{23} is stable during the simulation time of 200 ps.

Using the longer helices obtained during the unrestrained MD calculations as the basis for an estimate of the time averaged helix content by CD spectroscopy reduces the lower bound for the existence of full-length helices to 55%.

Comparison with Other Peptides—Secondary structure formation is reported for a number of small peptides (43, 61 and literature therein). Many of these small peptides are preferentially in α-helical conformation, although a few β-sheet-containing peptides are known (43). Observation of tertiary interactions, however, in monomeric, linear peptides as small as hPTH(1–37) or hPTH(1–34)[3] is unusual. In particular, conformations as rigid as the one we suggest for hPTH(1–37) on the basis of NMR spectroscopy, CD spectroscopy, and restrained as well as unrestrained molecular dynamics calculations, are rarely reported. Although it is difficult to point out any single reason for structure formation, it seems that the helix from Ser^{17} to Leu^{28} plays a crucial role in positioning the central Trp^{23} residue so that it may establish stable hydrophobic interactions with Leu^{15}. A similar example of a peptide showing tertiary interactions is the chimeric 25 amino acid peptide made of the core domain of equine infectious anemia virus transactivator (Tat) protein and the basic domain of human immunodeficiency virus Tat protein (42). This peptide forms a hydrophobic core that is structurally highly similar to the iden-

TABLE II
Energy contributions to the structure and deviations from standard geometry

E_{total}, total energy; E_{VDW}, van der Waals energy; E_{NOE}, effective NOE energy term resulting from a soft square-well potential function as described in the text. All calculations were carried out using the standard X-PLOR force field and energy terms. The values are mean values over 10 refined structures.

NOE and X-PLOR statistics	
No. of NOEs	
Total	520
$\|i-j\| = 0$	337
$\|i-j\| = 1$	109
$\|i-j\| = 2, 3, 4, 5$	69
$\|i-j\| > 5$	5
X-PLOR parameters after SA refinement	
rmsd from ideality	
NOEs (nm)	0.0118
angles (deg)	0.8452
bonds (nm)	0.0010
impr (deg)	0.6973
Average energies (kJ/mol)	
E_{NOE}	553.99
E_{VDW}	−2411,21
E_{total}	−1579,36
rmsd among backbone structures (nm)	
Met^{18}–Leu^{28}	0.052
His^{14}–Leu^{28}	0.069
Whole protein	0.526
NOE violations	≤5 (average: 1.7)

[3] U. Marx, K. Adermann, and W.-G. Forssmann, unpublished data.

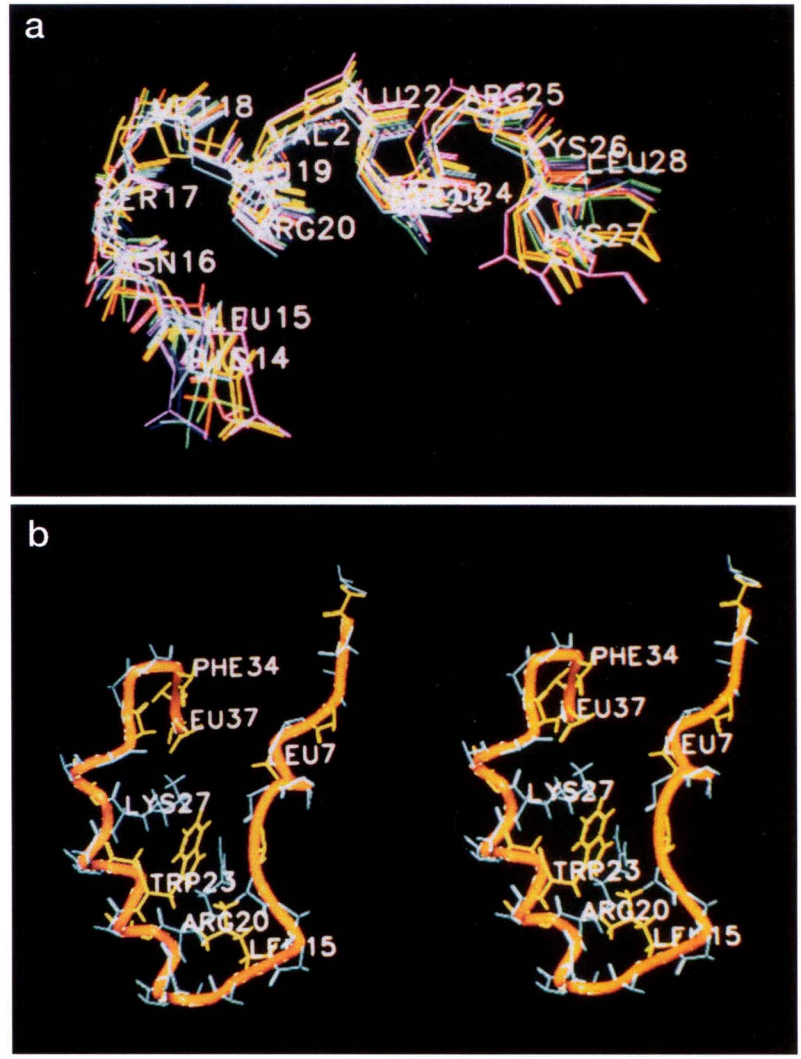

FIG. 6. *a*, best fit superposition of the peptide backbone atoms, amino acids His^{14} to Leu^{28}, of the 10 structures calculated and selected as described under "Material and Methods." *b*, stereo picture of a single structure selected from the set in *a*, with key residues labeled.

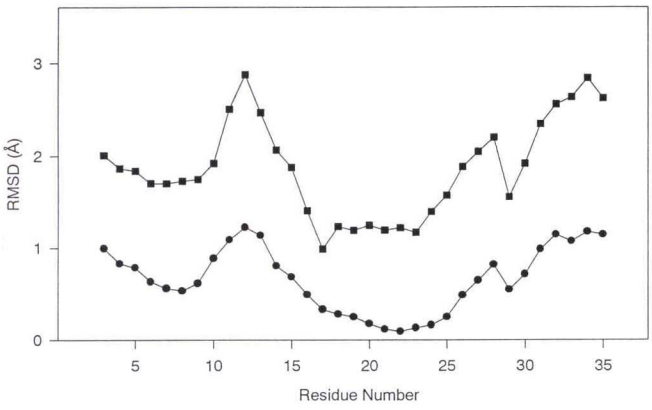

FIG. 7. **Plot of local rmsd values (59) *versus* amino acid sequence.** Backbone atoms of 5 amino acid segments of two structures were aligned and the pairwise rmsd values calculated. The procedure was performed for the 10 structures in Fig. 6*a*. The average backbone rmsd value is represented as a function of the sequence number of the residue in the window center.

tical sequence region in full-length Tat proteins (63, 64). In the peptide, this hydrophobic core is also flanked by an α-helix, but no long range interactions between core and helical region are observed.

hPTH Structure in TFE Containing versus TFE-free Solution—Comparing the results of the present structure determination close to physiological conditions with the secondary structures determined in TFE-containing solution (see, for example, (9, 13)), the following picture emerges: hPTH(1–34) does not display a well-defined tertiary structure in TFE-containing solution, a fact that is made obvious by the complete lack of long range NOEs in these studies. In contrast, in TFE-free solution the tertiary structure of the peptide is experimentally well defined by five long range NOEs between Leu^{15} and Trp^{23}. The turn region from His^{14} to Ser^{17} is stabilized by hydrophobic interactions. TFE with its lower polarity, $\epsilon = 26.7$ (23), has a strong tendency to overcome the hydrophobic stabilization energy. This adverse effect of TFE on hydrophobically stabilized protein structures was repeatedly observed (see, for example, Ref. 19).

hPTH(1–34) in TFE-free aqueous solution at pH 4.1 (10) shows a stable, extended NH_2-terminal α-helical region from Glu^4 to Lys^{13}, well defined by NOEs typical for stable α-helical structure. In contrast to these studies, we found a shorter helix from Gln^6 to His^9 by NOE-based restrained MD calculations (Ile^5 to Asn^{10} on the basis of subsequent unrestrained MD calculations as above), also indicated by the chemical shift index plot (Fig. 5) and the backbone NOE pattern (Fig. 6). In this respect, our results were in agreement with earlier NMR studies of hPTH(1–34) in TFE containing aqueous solution, where the NH_2-terminal helix ends with His^9 (9). We found a flexible hinge around Gly^{12} and a Gly^{12} $J_{NH\text{-}\alpha H}$ coupling constant of approximately 12 Hz, as observed earlier by others (9). The flexible region around Gly^{12} and Lys^{13} is necessary for the hormonal activity in an *in vitro* adenylate cyclase assay (65).

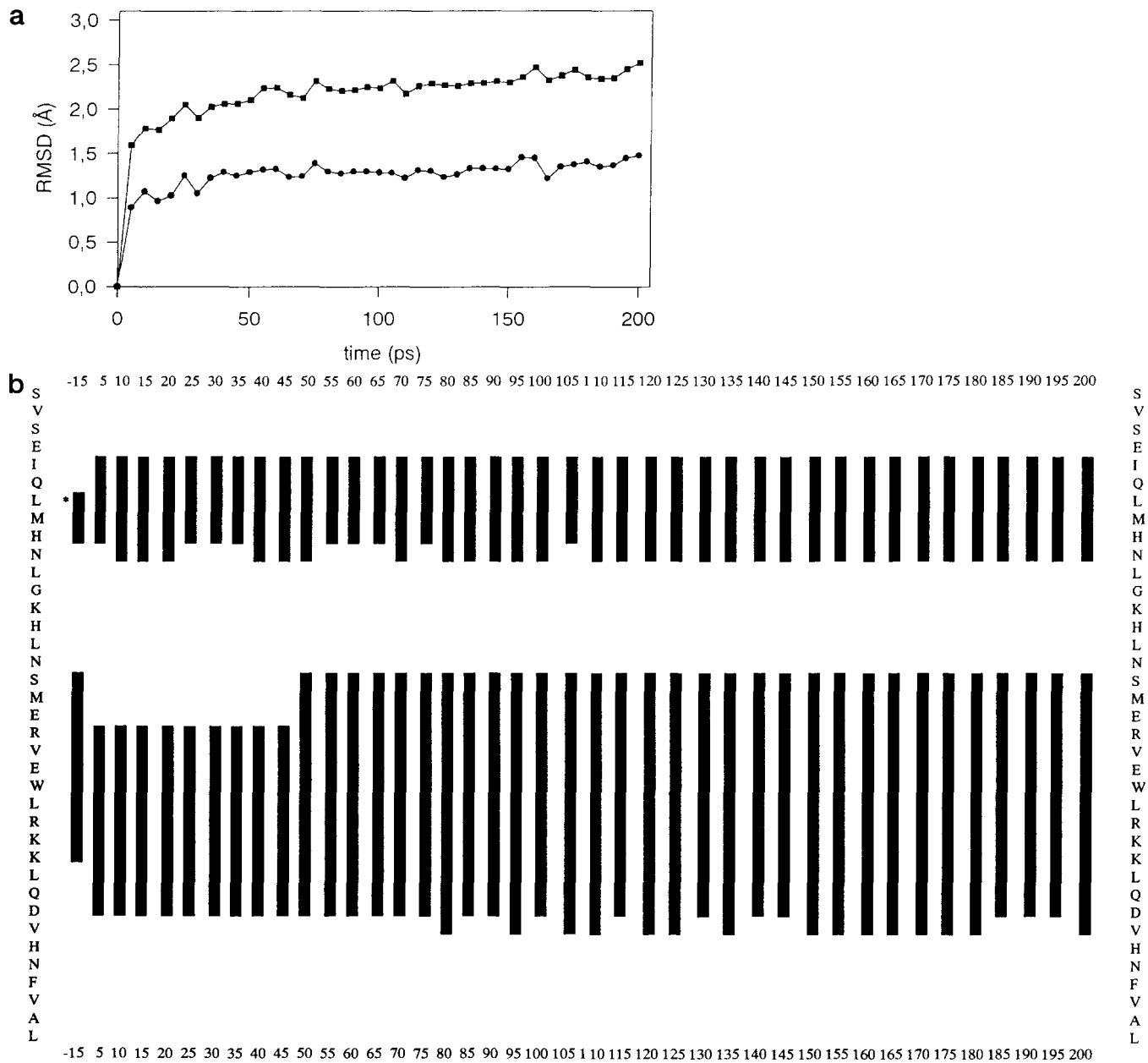

FIG. 8. *a*, backbone rmsd values of current structure *versus* starting structure during the 200-ps unrestrained molecular dynamics calculation. *Lower trace*, backbone heavy atoms; *upper trace*, all heavy atoms. *b*, time dependence of helix length during the 200-ps unrestrained molecular dynamics calculation. Helix structure content was evaluated by use of the DSSP program every 5 ps. The two helices are symbolized as *bars* in this figure.

This fact contrasts the notion of a long NH_2-terminal helix suggested earlier for hPTH(1–34) in TFE-free aqueous solution (10).

The structure of hPTH(1–37) showed a loop region from His^{14} to Ser^{17} followed by an α-helix from Ser^{17} to Leu^{28} as determined by NOE-based restrained MD calculations (Ser^{17} to Asp^{30} on the basis of subsequent unrestrained MD calculations as above). This region of the molecule forms a major part of the receptor binding domain (5, 6). The extent of the COOH-terminal helix is in good agreement with previous work in TFE containing as well as in TFE-free aqueous solution. Not only did the length of this helix in hPTH(1–37) vary in the unrestrained MD calculation, but also strong $\alpha N(i,i+1)$ NOEs were observed in this region. This helix thus seems to be in a less compact, more stretched conformation compared to the corresponding helix in hPTH(1–34) in TFE-containing aqueous solution.

The Ser^{17} to Leu^{28} helix observed in TFE-free solution is nearly an ideal helix when compared with the propensity of amino acids for certain positions in an α-helix (62). The N-cap is Asn^{16} or Ser^{17}, depending on the definition of the helix start. The positively charged side chains in the last turn are Arg^{25}, Lys^{26}, and Lys^{27}. Glu has a high probability to be at the second position COOH-terminal from the C-cap. These residues are represented by Glu^{29} and Asp^{30} in the case of hPTH(1–37). Hydrophobic amino acids are suggested to occupy positions +4 from the NH_2 terminus and −4 from the COOH terminus of the helix. Indeed, Val^{21} and Leu^{24} are at just these positions.

Ser^1, Val^2, $Ser^3$3, and Glu^4 of hPTH(1–37) are flexible and not included in any obvious secondary structural element. They also do not take part in hydrophobic interactions. Independent experiments, however, show that cleavage of hPTH between Val^2 and Ser^3 abolishes stimulation of cAMP-related activity (3). This indicates that the role of the NH_2-terminal amino acids cannot be explained on the basis of their local structure in the absence of receptor interaction.

Acknowledgment—The NDEE program was supplied by Franz Herrmann.

REFERENCES

1. Schlüter, K. D., Hellstern, H., Wigender, E., and Mayer, H. (1989) *J. Biol. Chem.* **264,** 11087–11092
2. Sömjen, D., Binderman, I., Schlüter, K. D., Wingender, E., Mayer, H., and Kaye, A. M. (1990) *Biochem. J.* **272,** 781–785
3. Potts, J. T., Kronenberg, H. M., and Rosenblatt, M. (1982) *Adv. Prot. Chem.* **35,** 323–396
4. Forssmann, W. G., Schulz-Knappe, P., Meyer, M., Adermann, K., Forssmann, K., Hock, D., and Aoki, A. (1993) in *Peptide Chemistry* 1992 (Yanaihara, N., ed) pp. 553–557, ESCOM, Leiden
5. Lopez-Hilker, S., Martin, K. J., Sugimoto, T., and Slatopolsky, E. (1992) *J. Lab. Clin. Med.* **119,** 738–743
6. Caulfield, M. P., McKee, R. L., Goldman, M. E., Doung, L. T., Fisher, J. E., Gay, C. T., deHaven, P. A., Levy, J. J., Roubini, E., Nutt, R. F., Chorev, M., and Rosenblatt, M. (1990) *Endocrinology* **127,** 83–87
7. Segre, G. V., Rosenblatt, M., Reiner, B. L., Mahaffey, J. E., and Potts, J. T. (1979) *J. Biol. Chem.* **254,** 6980–6986
8. Reeve, J., Meunier, P. J., Parson, J. A., Bernat, M., Bijovoet, O. L. M., Coupron, P., Edouard, C., Klenerman, L., Neer, R. M., Renier, J. C., Slovik, D., Vismans, F. J., and Potts, J. T. (1980) *Br. Med. J.* **280,** 1340–1344
9. Klaus, W., Dieckmann, T., Wray, V., Schomburg, D., Wingender, E., and Mayer, H. (1991) *Biochemistry* **30,** 6936–6942
10. Barden, J. A., and Cuthbertson, R. M. (1993) *Eur. J. Biochem.* **215,** 315–321
11. Strickland, L. A., Bozzato, R. P., and Kronis, K. A. (1993) *Biochemistry* **32,** 6050–6057
12. Chorev, M., and Rosenblatt, M. (1994) in *Structure-Function Analysis of Parathyroid Hormone and Parathyoid Hormone-related Protein* (Chorev, M., and Rosenblatt, M., eds) Raven Press, pp. 139–156, New York
13. Wray, V., Federau, T., Gronwald, W., Mayer, H., Schomburg, D., Tegge, W., and Wingender, E. (1994) *Biochemistry* **33,** 1684–1693
14. Barden, J. A., and Kemp, B. E. (1993) *Biochemistry* **32,** 7126–7132
15. Barden, J. A., and Kemp, B. E. (1989) *Eur. J. Biochem.* **184,** 379–394
16. Nelson, J. W., and Kallenbach, N. R. (1986) *Proteins* **1,** 211–217
17. Dyson, H. J., Merutka, G., Waltho, J. P., Lerner, R. A., and Wright, P. E. (1992) *J. Mol. Biol.* **226,** 795–817
18. Sönnichsen, F. D., van Eyk, J. E., Hodges, R. S., and Sykes, B. D. (1992) *Biochemistry* **31,** 8790–8798
19. Sticht, H., Willbold, D., Bayer, P., Ejchart, A., Herrmann, F., Rosin-Arbesfeld, R., Gazit, A., Yaniv, A., Frank, R., and Rösch, P. (1993) *Eur. J. Biochem.* **218,** 973–976
20. Lancelin, J. M., Bally, I., Arlaud, G. J., Blackledge, M., Gans, P., Stein, M., and Jacquot, J. P. (1994) *FEBS Lett.* **343,** 261–266
21. Morton, C. J., Simpson, R. J., and Norton, R. S. (1994) *Eur. J. Biochem.* **219,** 97–107
22. Buck, M., Radford, S. E., and Dobson, C. M. (1993) *Biochemistry* **32,** 669–678
23. Llinas, M., and Klein, M. P. (1975) *J. Am. Chem. Soc.* **97,** 4731–4737
24. Chou, P. Y., and Fasman, G. (1974) *Biochemistry* **13,** 222–245
25. Atherton, E., and Sheppard, R. C. (1989) *Solid Phase Peptide Synthesis: A Practical Approach*, JRL Press, Oxford
26. Yphantis, D. A. (1964) *Biochemistry* **3,** 297–317
27. Ernst, R. R. (1992) *Angew. Chemie, Int. Ed. Engl.* **104,** 817–852
28. Wüthrich, K. (1986) *NMR of Proteins and Nucleic Acids*, Wiley, New York
29. Brünger, A. (1993) *X-PLOR 3.1 Manual*, Yale University Press, New Haven
30. Brooks, B. R., Bruccoleri, R. E., Olafson, B. D., States, D. J., Swaminathan, S., and Karplus, M. (1983) *J. Comput. Chem.* **4,** 187–217
31. Jorgensen, W. L., Chandrasekhar, J., Madura, J. D., Impey, R. W., and Klein, M. L. (1983) *J. Chem. Phys.* **79,** 926–935
32. Powell, M. J. D. (1977) *Math. Progr.* **12,** 241–254
33. Berendsen, H. J. C., Postma, J. P. M., van Gunsteren, W. F., diNiola, A., and Haak, J. R. (1984) *J. Chem. Phys.* **81,** 3684–3690
34. Verlet, L. (1967) *Phys. Rev.* **159,** 98–103
35. van Gunsteren, W. F., and Berendsen, H. J. C. (1977) *J. Mol. Phys.* **34,** 1311–1327
36. Kabsch, W. S. C. (1983) *Biopolymers* **22,** 2577–2637
37. Morrisett, J. D., David, J. S. K., Pownall, H. J., and Gotto, A. M. (1973) *Biochemistry* **12,** 1290–1299
38. Greenfield, N., and Fasman, G. (1969) *Biochemistry* **8,** 4108–4116
39. Wishart, D. S., Sykes, B. D., and Richards, F. M. (1992) *Biochemistry* **31,** 1647–1651
40. Archer, S. J., Bax, A., Roberts, A. B., Sporn, M. B., Ogawa, Y., Piez, K. A., Weatherbee, J. A., Tsang, M. L., Lucas, R., Zheng, B. L., Wenker, J., and Torchia, D. A. (1993) *Biochemistry* **32,** 1164–1171
41. Willbold, D., Krüger, U., Frank, R., Rosin-Arbesfeld, R., Gazit, A., Yaniv, A., and Rösch, P. (1993) *Biochemistry* **32,** 8439–8445
42. Mujeeb, A., Bishop, K., Peterlin, B. M., Turck, C., Parslow, T. G., and James, T. L. (1994) *Proc. Natl. Acad. Sci. U. S. A.* **91,** 8248–8252
43. Dyson, H. J., and Wright, P. E. (1991) *Annu. Rev. Biophys. Biophys. Chem.* **20,** 519–538
44. Torda, A. E., Scheek, R. M., and van-Gunsteren, W. F. (1990) *J. Mol. Biol.* **214,** 223–235
45. Bradley, E. K., Thomason, J. F., Cohen, F. E., Kosen, P. A., and Kuntz, I. D. (1990) *J. Mol. Biol.* **215,** 607–622
46. Wüthrich, K., Billeter, M., and Braun, W. (1984) *J. Mol. Biol.* **180,** 715–740
47. Weiss, M. A., Ellenberger, T., Wobbe, C. R., Lee, J. P., Harrison, S. C., and Struhl, K. (1990) *Nature* **347,** 575–578
48. Saudek, V., Pastore, A., Castiglione-Morelli, A., Frank, R., Gausepohl, H., Gibson, T., Weih, F., and Rösch, P. (1991) *Protein Eng.* **4,** 3–10
49. Saudek, V., Pastore, A., Morelli, M. A., Frank, R., Gausepohl, H., and Gibson, T. (1991) *Protein Eng.* **4,** 519–529
50. Omichinski, J. G., Clore, G. M., Appella, E., Sakaguchi, K., and Gronenborn, A. M. (1990) *Biochemistry* **29,** 9324–9334
51. Hard, T., Kellenbach, E., Boelens, R., Kaptein, R., Dahlman, K., Carlstedt-Duke, J., Freedman, L. P., Maler, B. A., Hyde, E. I., Gustafsson, J. A., and Yamamoto, K. R. (1990) *Biochemistry* **29,** 9015–9023
52. Schwabe, J. W., Neuhaus, D., and Rhodes, D. (1990) *Nature* **348,** 458–461
53. Klevit, R. E., Herriott, J. R., and Horvath, S. J. (1990) *Proteins* **7,** 215–226
54. Dyson, J. H., Rance, M., Houghten, R. A., Wright, P. E., and Lerner, R. A. (1988) *J. Mol. Biol.* **201,** 201–217
55. Saudek, V., Pasley, H. S., Gibson, T., Gausepohl, H., Frank, R., and Pastore, A. (1991) *Biochemistry* **30,** 1310–1317
56. Junius, F. K., Weiss, A. S., and King, G. F. (1993) *Eur. J. Biochem.* **214,** 415–424
57. Woody, R. W. (1994) in *Circular Dichroism* (Nakanishi, K., Berova, N., and Woody, R. W., eds) pp. 473–496, VCH Publishers, Weinheim
58. Yang, J. T., Wu, C.-S. C., and Martinez, H. M. (1986) in *Calculation of Protein Conformation from Circular Dichroism* (Yang, J. T., Wu, C.-S. C., and Martinez, H. M., eds) pp. 208–269, Academic Press, Inc., San Diego
59. Wagner, G., Braun, W., Havel, T. F., Schaumann, T., Go, N., and Wüthrich, K. (1987) *J. Mol. Biol.* **196,** 611–639
60. Van-Buuren, A. R., and Berendsen, H. J. (1993) *Biopolymers* **33,** 1159–1166
61. Merutka, G., Morikis, D., Bruschweiler, R., and Wright, P. E. (1993) *Biochemistry* **32,** 13089–13097
62. Richardson, J. S., and Richardson, D. C. (1988) *Science* **240,** 1648–1652
63. Willbold, D., Rosin-Arbesfeld, R., Sticht, H., Frank, R., and Rosch, P. (1994) *Science* **264,** 1584–1587
64. Bayer, P., Kraft, M., Westendorp, M., Frank, R., and Rösch, P. (1995) *J. Mol. Biol.* **247,** 529–535
65. Chorev, M., Goldman, M. E., McKee, R. L., Roubini, E., Levy, J. J., Gay, C. T., Reagan, J. E., Fisher, J. E., Caporale, L. H., Golub, E. E., Caulfield, M. P., Nutt, R. F., and Rosenblatt, M. (1990) *Biochemistry* **29,** 1580–1586